Universität Karlsruhe (TH)
Forschungsuniversität • gegründet 1825

Institut für Mechanik

On “Solid-Shell” Elements with Linear and Quadratic Shape Functions for Small and Large Deformations

M. Harnau, K. Schweizerhof, R. Hauptmann
Universität Karlsruhe, Institut für Mechanik

2000

Institut für Mechanik
Kaiserstr. 12, Geb. 20.30
76128 Karlsruhe
Tel.: +49 (0) 721/ 608-2071
Fax: +49 (0) 721/ 608-7990
E-Mail: ifm@uni-karlsruhe.de
www.ifm.uni-karlsruhe.de

ON 'SOLID-SHELL' ELEMENTS WITH LINEAR AND QUADRATIC SHAPE FUNCTIONS FOR SMALL AND LARGE DEFORMATIONS

M. Harnau*, K. Schweizerhof*, and R. Hauptmann

*Institut für Mechanik, Universität Karlsruhe, 76128 Karlsruhe, Germany

Key words: Solid-Shell elements, large deformations, volumetric locking, trapezoidal locking

Abstract. *The well known Solid-Shell concept was originally developed as 'four-node type' elements with trilinear shape functions [20], [24] and [15]. Every 'nodal point' consists of one node on the upper surface and one node on the lower surface with three displacement degrees of freedom each. In this contribution these four-node respectively eight-node elements are extended to nine-node respectively eighteen-node elements with biquadratic-linear shape functions, and investigated for their capabilities for applications in the large deformation regions.*

The major advantage of the 'nine-node type' elements with the biquadratic-linear shape functions is mainly that a much better geometrical approximation especially for curved shell structures becomes possible. This can be shown with different numerical examples.

For the biquadratic-linear as well as for the trilinear elements different locking effects appear. These locking effects will be discussed and a summary of methods to overcome the locking problems will be presented. However, as a consequence problems occur in the large deformation regime, such that under some types of loading the trilinear elements as well as the biquadratic-linear elements become unstable, indicated by negative eigenvalues of the tangential stiffness matrix. This topic is discussed in detail.

1 INTRODUCTION

With the 'Solid-Shell' concept a shell element formulation was developed, to overcome some limits of the well-known degeneration concept. Using nodes at upper and lower surface and using only displacement degrees of freedom allows general three-dimensional material laws to be implemented, thus strains and stresses in thickness direction can be calculated properly. In addition, the treatment of rotations can be avoided completely and the transition to full 3D-continuum parts is directly possible.

The assumed natural strain (ANS) method proposed by Bathe and Bucalem [9], already taken in a similar fashion [1] for the 'four-node type' element to avoid transverse shear locking, is used for the 'nine-node type' elements to avoid first transverse shear locking and second the additionally appearing membrane locking for elements with higher order shape functions. The problem of thickness locking is resolved by enhancing the normal strain in thickness direction with a linear extension using the EAS-method [5] and [24], or alternatively by increasing the order of interpolation for the displacements in thickness direction over the thickness using an additional degree of freedom [14].

Considering nearly incompressible material behavior, like rubber elasticity or metal plasticity, the problem of incompressibility locking appears. A rather efficient possibility - among others as e.g. the EAS-method [5] - to resolve this problem is to use a lower order of integration for the volumetric parts of the stress tensor and the tangent moduli tensor, the so called selective reduced integration (SRI). The selective reduced integration of volumetric parts indeed presumes that a isochoric-volumetric material behavior is implemented.

Under some types of loading the trilinear elements as well as the biquadratic-linear elements become unstable at a certain level of loading. Then the well known hourglassing phenomenon appears if e.g. the EAS-method is used for homogenous compression/tension states. Such investigations lead to the result that under some boundary conditions similar effects also appear when only the ANS-method is included presuming a large deformation state is given.

Another locking effect known for elements with linear and quadratic shape functions is the problem of so called trapezoidal locking. This effect is only found in structures where the directors of the element edges are not vertical to the mid-layer. One method to resolve this problem is using an assumed strain interpolation of the normal strain in thickness direction as performed in [27] resp. in [2] and [3], where it was proposed to avoid artificial thickness straining.

2 BASIC RELATIONS OF THE SOLID-SHELL CONCEPT

In this section the basic features of the solid-shell concept are briefly reviewed. For a more detailed explanation we refer to [16]. The initial geometry $\boldsymbol{X}$ is described as

$$\boldsymbol{X}(\xi,\eta,\zeta) = \frac{1}{2}\,[\,(1+\zeta)\boldsymbol{X}_u(\xi,\eta)\;+\;(1-\zeta)\boldsymbol{X}_l(\xi,\eta)\,], \tag{1}$$

the displacements $\boldsymbol{u}$ of the three-dimensional shell are approximated as follows:

$$\boldsymbol{u}(\xi,\eta,\zeta) \;=\; \boldsymbol{T}^{-1}(\xi,\eta)\,\boldsymbol{\Theta}(\zeta) \left[\begin{array}{cc|c} \boldsymbol{T}(\xi,\eta) & \boldsymbol{0}_{3\times3} & \boldsymbol{0}_{3\times n} \\ \boldsymbol{0}_{3\times3} & \boldsymbol{T}(\xi,\eta) & \boldsymbol{0}_{3\times n} \\ \hline \boldsymbol{0}_{n\times3} & \boldsymbol{0}_{n\times3} & \boldsymbol{1}_{n\times n} \end{array}\right] \left(\begin{array}{c} \boldsymbol{u}_u(\xi,\eta) \\ \boldsymbol{u}_l(\xi,\eta) \\ \hline \boldsymbol{\beta}(\xi,\eta) \end{array}\right). \tag{2}$$

The indices u, l refer to the geometry resp. the displacements of the upper/lower surface nodes. The matrix $\boldsymbol{T}$ is used for the transformation from global cartesian coordinates (x, y, z) to local orthonormal coordinates (ξ, η, ζ) aligned to the geometry of the shell-mid-surface. The matrix $\boldsymbol{T}^{-1}$ allows the inverse transformation. It should be mentioned, that in equations (1) and (2) the values $\boldsymbol{X}$ and $\boldsymbol{u}$ as well as their discrete nodal values are given with respect to global cartesian coordinates. In contrast, the additional degrees of freedom $\boldsymbol{\beta}$ belonging to a hierarchical thickness interpolation are given with respect to the local thickness coordinate. In equations (1) and (2) the approximation in in-plane direction is decoupled from the approximation in thickness direction. The upper shell surface (index u) and the lower shell surface (index l) contain the in-plane approximation (local convective coordinates ξ and η). All terms which are dependent on ζ (local thickness coordinate) describe the approximation in thickness direction. Choosing a linear interpolation matrix

$$\boldsymbol{\Theta}(\zeta) = \frac{1}{2}\left[\begin{array}{cccccc} 1+\zeta & 0 & 0 & 1-\zeta & 0 & 0 \\ 0 & 1+\zeta & 0 & 0 & 1-\zeta & 0 \\ 0 & 0 & 1+\zeta & 0 & 0 & 1-\zeta \end{array}\right]. \tag{3}$$

in thickness direction, the displacement approximation (2) is identical to the geometry approximation (1). Then, making use of the relation $\boldsymbol{T}^{-1}\boldsymbol{T} = \boldsymbol{1}$, no transformation matrix is required. Furthermore, no additional degrees of freedom $\boldsymbol{\beta}$ are necessary, i.e. the last line and the last column of the matrix-vector product in equation (2) can be omitted. However, with higher order interpolation in thickness direction, using additional degrees of freedom $\boldsymbol{\beta}$ the transformation matrix $\boldsymbol{T}$ is needed.

The geometry in the current configuration is given by the relation $\boldsymbol{x} = \boldsymbol{X} + \boldsymbol{u}$. Thus, the displacement gradient, deformation gradient and the Green-Lagrange strain tensor

$$\boldsymbol{H} = \frac{\partial \boldsymbol{u}}{\partial \boldsymbol{X}}, \qquad \boldsymbol{F} = \frac{\partial \boldsymbol{x}}{\partial \boldsymbol{X}} \qquad \text{and} \qquad \boldsymbol{E} = \frac{1}{2}\left(\boldsymbol{F}^T\boldsymbol{F} - \boldsymbol{1}\right) \tag{4}$$

can be computed. The 2. Piola-Kirchhoff stress tensor $\boldsymbol{S}$ and the tangent moduli tensor $\mathbb{C} = \partial\boldsymbol{S}/\partial\boldsymbol{E}$ result from the material law. The latter is based on a so-called strain-driven algorithm also known as 'algorithmic box'. In contrast to the degenerated shell concept the fully three-dimensional strain tensor and stress tensor are applied, i.e. strains and stresses in thickness direction are admitted and any general three-dimensional material law can be used without modification.

It should be mentioned, that the basic relations introduced above hold for both element types considered in the following sections: elements with bilinear and elements with biquadratic interpolation in in-plane direction.

3 BILINEAR ELEMENTS

First solid-shell elements with bilinear interpolation in in-plane direction are discussed, i.e. the upper shell surface and the lower shell surface are discretized each by 4 nodes. This involves bilinear interpolation for the geometry $\boldsymbol{X}_u(\xi,\eta)$, $\boldsymbol{X}_l(\xi,\eta)$ and for the displacements $\boldsymbol{U}_u(\xi,\eta)$, $\boldsymbol{U}_l(\xi,\eta)$ as well as for the additional displacements $\boldsymbol{\beta}(\xi,\eta)$.

3.1 Transverse shear locking

As known from degenerated shell elements transverse shear locking appears. A removal is achieved with the assumed natural strain method interpolating the transverse shear strains as proposed by Bathe and Dvorkin [1]:

$$\begin{aligned} E^{ANS}_{\xi\zeta}(\eta,\zeta) &= \frac{1}{2}[1-\eta]\; E_{\xi\zeta}(\xi=0,\eta=-1,\zeta) + \frac{1}{2}[1+\eta]\; E_{\xi\zeta}(\xi=0,\eta=+1,\zeta), \\ E^{ANS}_{\eta\zeta}(\xi,\zeta) &= \frac{1}{2}[1-\xi]\; E_{\eta\zeta}(\xi=-1,\eta=0,\zeta) + \frac{1}{2}[1+\xi]\; E_{\eta\zeta}(\xi=+1,\eta=0,\zeta). \end{aligned} \tag{5}$$

For brevity no further details on this approach are discussed here. For the proper incorporation into the solid-shell concept we refer to [15].

3.2 Membrane locking

Due to the coupling of the normal strains with the shear strains in in-plane direction membrane locking may occur in particular for larger aspect ratios of the elements. To suppress this locking the EAS approach originally proposed by Simo and Rifai [25] is applied for the approximation of the in-plane strains (index ip):

$$\begin{aligned} \boldsymbol{E}^{EAS}_{ip} &= \begin{pmatrix} E_{11} \\ E_{22} \\ 2E_{12} \end{pmatrix}^{EAS} = \boldsymbol{E}^{c}_{ip} + \boldsymbol{M}\boldsymbol{\alpha} \\ &= \boldsymbol{E}^{c}_{ip} + \frac{1}{\det \boldsymbol{J}} \begin{bmatrix} t_{11}^2 & t_{12}^2 & t_{11}t_{12} \\ t_{21}^2 & t_{22}^2 & t_{21}t_{22} \\ 2t_{11}t_{21} & 2t_{12}t_{22} & t_{11}t_{22}+t_{12}t_{21} \end{bmatrix} \widehat{\boldsymbol{M}}\boldsymbol{\alpha}. \end{aligned} \tag{6}$$

The vector $\boldsymbol{E}_{ip}$ contains the in-plane Green-Lagrange strains, where $\boldsymbol{E}^{c}_{ip}$ are the strains compatible to the displacements. The factors

$$t_{mn} = \boldsymbol{G}_m(\xi,\eta,\zeta)\cdot\boldsymbol{G}^n(0,0,0) \qquad \text{with} \quad m,n=1,2 \tag{7}$$

are used to transform the enhanced strains to the covariant coordinate system at the element mid-point which is necessary to obtain unique values for the parameters α_i. The parameters α_i can be considered as element variables resulting from so-called incompatible approximations between the elements. The vectors $\boldsymbol{G}_m$ and $\boldsymbol{G}^n$ in equation (7) are the base vectors of the covariant respectively contravariant coordinate system.

The matrix $\widehat{\boldsymbol{M}}$ is chosen according to Simo/Rifai [25]

$$\widehat{\boldsymbol{M_1}} = \begin{bmatrix} \xi & 0 & 0 & 0 \\ 0 & \eta & 0 & 0 \\ 0 & 0 & \xi & \eta \end{bmatrix}. \tag{8}$$

3.3 Thickness locking

Solid-shell elements suffer from so-called thickness locking, if a linear displacement assumption in thickness direction is used, see e.g. Verhoeven [28], Braun [5], Hauptmann [16]. For a short discussion here the standard St.-Venant-Kirchhoff material law is taken. If the stress-strain relation for $S^{\zeta\zeta}$ is considered, the strain $E_{\zeta\zeta}$, which is constant in thickness direction, is coupled via the Poisson-ratio with the strains $E_{\xi\xi}$, $E_{\eta\eta}$, which vary linearly in thickness direction. Thus, in pure bending situations instead of $S^{\zeta\zeta} = 0$ a linear $S^{\zeta\zeta}$ stress distribution would result, leading to an overly stiff behavior. To overcome this thickness locking an additional $E_{\zeta\zeta}$ strain with linear distribution in thickness direction must be introduced. In the following two different approaches are considered.

Approach 1: As suggested in [14] for multi-director elements, an additional quadratic term is introduced into the interpolation matrix (3) in thickness direction:

$$\bar{\boldsymbol{\Theta}}(\zeta) = \frac{1}{2} \left[\begin{array}{cccccc|c} 1+\zeta & 0 & 0 & 1-\zeta & 0 & 0 & 0 \\ 0 & 1+\zeta & 0 & 0 & 1-\zeta & 0 & 0 \\ 0 & 0 & 1+\zeta & 0 & 0 & 1-\zeta & 1-\zeta^2 \end{array}\right]. \tag{9}$$

Thus one additional degree of freedom β at each node belonging to a hierarchical thickness interpolation is employed ($n = 1$ in equation (2)), which is identical to a quadratic displacement approximation, and consequently a linear $E_{\zeta\zeta}$ strain approximation in thickness direction is achieved. This additional degree of freedom is usually treated as global nodal degree of freedom.

Approach 2: The constant normal strain in thickness direction is enhanced with a linear extension over the thickness and bilinear in in-plane direction according to the EAS method, as proposed in [24] and [5]:

$$E_{\zeta\zeta}^{EAS} = E_{\zeta\zeta}^{c} + \tilde{\boldsymbol{M}}\tilde{\boldsymbol{\alpha}} = E_{\zeta\zeta}^{c} + \frac{1}{\det \boldsymbol{J}}\, \zeta \begin{bmatrix} 1 & \xi & \eta & \xi\eta \end{bmatrix} \begin{pmatrix} \tilde{\alpha}_1 \\ \tilde{\alpha}_2 \\ \tilde{\alpha}_3 \\ \tilde{\alpha}_4 \end{pmatrix}. \tag{10}$$

Herein $E_{\zeta\zeta}^{c}$ denotes the constant thickness strain which is compatible to the displacements, $\det \boldsymbol{J}$ is the determinant of the Jacobian of the isoparametric map, calculated at each Gauss point, and the vector $\tilde{\boldsymbol{\alpha}}$ consists of incompatible parameters, so-called element variables, that are condensed out on element level.

3.4 Volumetric locking

If nearly incompressible material behavior is considered, e.g. rubber elasticity or metal plasticity, the elements often suffer from so - called volumetric locking. Here two approaches are considered. The objective of both approaches is to fulfill the incompressibility

condition

$$\det \boldsymbol{F} = \det(\mathbf{1} + \boldsymbol{H}) = 1 + \mathrm{tr}\boldsymbol{H} + \frac{1}{2}[(\mathrm{tr}\boldsymbol{H})^2 - \mathrm{tr}(\boldsymbol{H}^2)] + \det \boldsymbol{H} = 1, \tag{11}$$

within the full range of the nonlinear behavior. The first approach is based on the use of different numerical integration points, where the constraint (11) is only fulfilled for a special material law. The second approach is based on the fulfillment of the linear part of eqn. (11) at the standard integration points and neglects the higher order terms.

Approach 1: If an isochoric-volumetric decoupled material behavior can be assumed, the stress tensor and tangent moduli tensor can be split into deviatoric and volumetric parts:

$$\boldsymbol{S} = \boldsymbol{S}^{\mathrm{dev}} + \boldsymbol{S}^{\mathrm{vol}} \qquad \text{and} \qquad \mathbb{C} = \mathbb{C}^{\mathrm{dev}} + \mathbb{C}^{\mathrm{vol}}.$$

It is well known [19] and [26] that the assumption of a constant dilatation is necessary to remove the artificial volumetric locking effect. Thus all integrals of the stiffness matrix and internal force vector containing volumetric terms $\boldsymbol{S}^{\mathrm{vol}}$ and $\mathbb{C}^{\mathrm{vol}}$ are numerically integrated with an order of integration below the standard order, the so called selective reduced integration (SRI):

$$\int_{\mathrm{sri}} (\ldots)^{\mathrm{vol}} dV \qquad \text{instead of} \qquad \int_{\mathrm{full}} (\ldots)^{\mathrm{vol}} dV. \tag{12}$$

For solid-shells the SRI for the volumetric terms is employed only in in-plane direction, i.e. 1×1 integration instead of 2×2 (full) integration, while the integration in thickness direction remains unchanged. Further details are given in [11] and [17]. The disadvantage of such an approach is the restriction to an isochoric-volumetric decoupled material law.

Approach 2: In the theory of small strains the incompressibility constraint (11) reduces to

$$\mathrm{tr}\boldsymbol{E} = 0. \tag{13}$$

Using the concepts to avoid thickness locking (see section 3.3) the interpolation of all normal strains is identical in ζ direction. In order to investigate the approximation of the normal strains in in-plane direction they are rewritten in terms of the local ξ and η coordinates:

$$\begin{aligned} E_{\xi\xi} &= a_1 + a_2\eta, \\ E_{\eta\eta} &= b_1 + b_2\xi, \\ E_{\zeta\zeta} &= c_1 + c_2\xi + c_3\eta + c_4\xi\eta. \end{aligned} \tag{14}$$

For a detailed discussion of this aspect for plane elements we refer to [4]. It is obvious that for the solid shells the counterparts ξ and $\xi\eta$ respectively η and $\xi\eta$ of the normal strain in thickness direction $E_{\zeta\zeta}$ are missing for the in-plane strains $E_{\xi\xi}$ and $E_{\eta\eta}$. The volumetric locking can be reduced by adopting the EAS approach as shown in eqn. (6) in combination with the matrix

$$\widehat{\boldsymbol{M_2}} = \left[\begin{array}{cccc|cc} \xi & 0 & 0 & 0 & \xi\eta & 0 \\ 0 & \eta & 0 & 0 & 0 & \xi\eta \\ 0 & 0 & \xi & \eta & 0 & 0 \end{array}\right] . \tag{15}$$

Then condition (13) can be fulfilled. The enhancement in (15) is an extension of the enhancement (8). The advantage of approach 2 is that no restrictions concerning material laws are imposed.

It is rather obvious that due to the nonlinear terms for $\boldsymbol{H}$ in equation (11) the compressibility constraint cannot be fulfilled exactly with the EAS approach of equation (15). Thus it is a rather interesting aspect to show how large the influence of the nonlinear terms on the volumetric locking is for different problems. This can be e.g. numerically checked by employing the isochoric-volumetric decoupled material and the selective reduced integration for the inplane terms as a further option.

3.5 Trapezoidal locking

The phenomenon of trapezoidal locking appears for distorted element meshes, presuming the directors at the element edges - resp. the vector pointing from the lower node to the upper node of the edges - are not in a 90 degree angle to the element mid-surface. These oblique directors activate incompatible normal strains in thickness direction and may lead to locking. To a avoid this locking behavior an assumed transverse normal strain distribution was proposed by [27]. A closer look shows that it is very close to the suggestions in [2] and [3] to avoid artificial thickness straining. Thus the strains resulting from the displacements in thickness direction are evaluated at the element edges and a bilinear strain interpolation is achieved using the standard Lagrange shape functions $N_i(\xi,\eta) = \frac{1}{4}(1+\xi_i\xi)(1+\eta_i\eta),\ i = 1\ldots 4$, which leads to the following equation:

$$\begin{aligned} \tilde{\varepsilon}_{zz} \;=\; & N_{1(\xi,\eta)}\,\varepsilon_{zz(\xi_1=-1,\eta_1=-1)} + N_{2(\xi,\eta)}\,\varepsilon_{zz(\xi_2=1,\eta_2=-1)} + N_{3(\xi,\eta)}\,\varepsilon_{zz(\xi_3=1,\eta_3=1)} + \\ & N_{4(\xi,\eta)}\,\varepsilon_{zz(\xi_4=-1,\eta_4=1)} \ . \end{aligned} \tag{16}$$

The strains ε_{zz} are the normal strains in thickness direction refering to a local cartesian coordinate system with the z-axis vertical to the mid surface.

3.6 Algorithmic treatment of the material law

In section 2 the material law is interpreted using a strain-driven algorithmic box. If the Green-Lagrange strain tensor $\boldsymbol{E}$ is the driving strain tensor, then the modified strains $\boldsymbol{E}^*$ resulting from the assumed and enhanced strain concept (5), (10), (6), (15) and (16) are the input values of the algorithmic box. If the deformation gradient $\boldsymbol{F}$ is the driving tensor, then the modified deformation gradient

$$\boldsymbol{F}^* = \boldsymbol{R}\boldsymbol{U}^* \quad \text{with} \quad \boldsymbol{R} = \boldsymbol{F}\boldsymbol{U}^{-1} \quad \text{and} \quad \boldsymbol{U}^* = (2\boldsymbol{E}^* + \boldsymbol{1})^{1/2}$$

has to be computed consistently to the modified strains $\boldsymbol{E}^*$. Then $\boldsymbol{F}^*$ can be directly used as input of the algorithmic material box (see also Eberlein [12] and Doll [10]). These

assumptions allow to treat the mixed type elements concerning large deformations in an identical fashion as a pure displacement approach independently of the type of strain interpolation.

3.7 Nomenclature

For a better distinction of the developed bilinear elements a special nomenclature is introduced, see Table **1**. The structure of the notation is 'xxx3Dyyy', where 'xxx' represents the in-plane approximation and 'yyy' represents the thickness approximation. The abbreviation '3D', which is identical for all elements, indicates the three-dimensionality of the solid-shell formulation. An additional extension -rv denotes selective **r**educed integration of the **v**olumetric terms following eqn. (12), the extension -at denotes an **a**ssumed strain interpolation of the **t**ransverse normal strain after equation (16).

Elementname	bilinear in-plane approximation	thickness approximation
ANS3Dq	(5)	(9)
ANS3DEAS	(5)	(3), (10)
EAS3DEAS	(5), (6) with (8)	(3), (10)
eas3DEAS	(5), (6) with (15)	(3), (10)
eas3Dq	(5), (6) with (15)	(9)
xxx3Dyyy-rv	selective reduced integration of volumetric term, see (12)	
xxx3Dyyy-at	assumed strain interpolation of the transverse normal strain (16)	

Table 1: Nomenclature of the bilinear elements.

4 BIQUADRATIC ELEMENTS

Within this section only the additions concerning solid-shell elements with biquadratic Lagrangian interpolation in in-plane direction are presented. The upper shell surface and the lower shell surface are discretized each using 9 nodes.

4.1 Transverse shear locking and membrane locking

To suppress transverse shear locking and membrane locking the assumed natural strain method as proposed by Bathe and Bucalem [9] is employed. The assumed membrane strains

$$
\begin{aligned}
E^{ANS}_{\xi\xi}(\xi,\eta,\zeta) &= \sum_{i=1}^{3}\sum_{j=1}^{2} P_i(\eta)Q_j(\xi)\ E_{\xi\xi}(\xi_j,\eta_i,\zeta)\ , \\
E^{ANS}_{\eta\eta}(\xi,\eta,\zeta) &= \sum_{i=1}^{3}\sum_{j=1}^{2} P_i(\xi)Q_j(\eta)\ E_{\eta\eta}(\xi_i,\eta_j,\zeta)\ , \\
E^{ANS}_{\xi\eta}(\xi,\eta,\zeta) &= \sum_{i=1}^{2}\sum_{j=1}^{2} Q_i(\xi)Q_j(\eta)\ E_{\xi\eta}(\xi_i,\eta_j,\zeta)
\end{aligned}
\tag{17}
$$

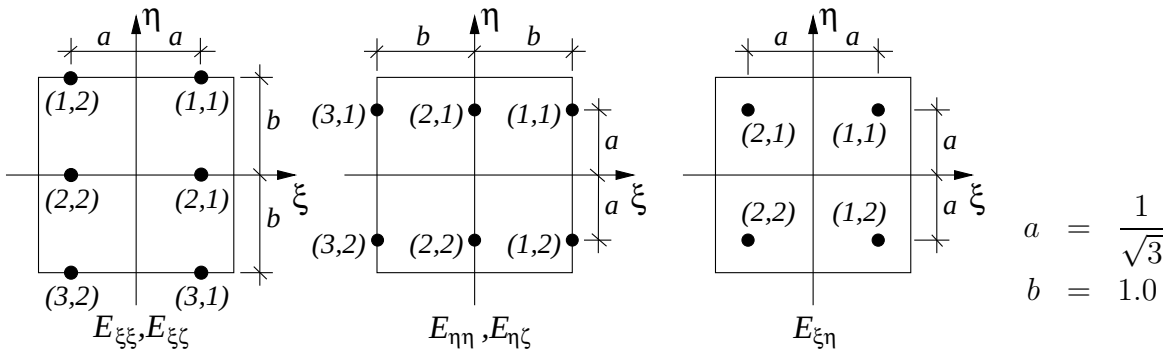

Figure 1: Evaluation points for strain interpolation functions

and the assumed transverse shear strains

$$
\begin{aligned}
E^{ANS}_{\xi\zeta}(\xi,\eta,\zeta) &= \sum_{i=1}^{3}\sum_{j=1}^{2} P_i(\eta)Q_j(\xi)\, E_{\xi\zeta}(\xi_j,\eta_i,\zeta)\ , \\
E^{ANS}_{\eta\zeta}(\xi,\eta,\zeta) &= \sum_{i=1}^{3}\sum_{j=1}^{2} P_i(\xi)Q_j(\eta)\, E_{\eta\zeta}(\xi_i,\eta_j,\zeta)
\end{aligned}
\tag{18}
$$

result from the interpolation

$$
\begin{aligned}
&P_1(\theta) = \frac{\theta}{2}(\theta+1), \qquad P_2(\theta) = 1-\theta^2, \qquad P_3(\theta) = \frac{\theta}{2}(\theta-1), \\
&Q_1(\theta) = \frac{1}{2}(1+\sqrt{3}\theta), \quad Q_2(\theta) = \frac{1}{2}(1-\sqrt{3}\theta) \quad \text{with } \theta = \xi,\eta
\end{aligned}
$$

of the compatible strains at the points

$$
\theta_{1,2,3} = +1, 0, -1 \text{ and } \theta_{1,2} = +\frac{1}{\sqrt{3}}, -\frac{1}{\sqrt{3}}.
$$

As only minor adaptations are performed for the solid shell concept, for brevity reasons no further details on this approach are discussed here.

An alternative for improving the membrane behavior would be to use enhanced strains also for the membrane direction as proposed by Bischoff [6] and [7] in analogy as for the elements with linear interpolation. However, as the effort required for a static condensation increases with the number of parameters in addition to the effort needed for the handling of these rather large number of parameters in a nonlinear analysis, this alternative is not followed here.

4.2 Thickness locking

If the linear interpolation matrix eqn.(3) in thickness direction is used, thickness locking may appear. This phenomenon described in section 3.3 is identical for the solid elements

based on bilinear and biquadratic shape functions. Both approaches, following eqn.(9) and eqn.(10), to avoid thickness locking can be used for the biquadratic solid-shells.

Approach 1: The hierarchical interpolation is performed with an additional degree of freedom at each location of the nine in-plane nodes, thus a biquadratic inplane interpolation is used for these hierarchical degrees of freedom in analogy to the displacements.

Approach 2: As the corresponding interpolation to avoid thickness locking with the EAS approach contains also quadratic terms in ξ and η, nine parameters are necessary for a consistent enhancement:

$$\begin{aligned} E_{\zeta\zeta}^{EAS} &= E_{\zeta\zeta}^{c} + \tilde{\boldsymbol{M}}\tilde{\boldsymbol{\alpha}} \\ &= E_{\zeta\zeta}^{c} + \frac{1}{\det \boldsymbol{J}}\,\zeta\, t_{33}^{2} \left[\begin{array}{ccccccccc} 1 & \xi & \eta & \xi\eta & \xi^2 & \eta^2 & \xi^2\eta & \xi\eta^2 & \xi^2\eta^2 \end{array}\right] \left(\begin{array}{c} \tilde{\alpha}_1 \\ \vdots \\ \tilde{\alpha}_9 \end{array}\right). \end{aligned} \tag{19}$$

The arguments are identical to those for the bilinear elements. The factor

$$t_{33} = \boldsymbol{G}_3(\xi,\eta,\zeta)\cdot\boldsymbol{G}^3(0,0,0) \tag{20}$$

is, in analogy to eqn.(6), needed for a transformation of the enhanced strains to the covariant coordinate system at the element mid-point.

It is obvious that the number of parameters for the incompatible strains is increasing considerably. Thus the efficiency of the biquadratic solid shell elements is considerably affected, as the static condensation requires an inversion of a 9/9-matrix per element, already for this part of the EAS approach.

4.3 Volumetric locking

To reduce the volumetric locking behavior within this study only the selective reduced integration of the volumetric terms is employed for the biquadratic elements, as introduced as first approach in section 3.4. The selective reduced integration (12) is applied in in-plane direction. However contrary to the bilinear elements SRI means 2×2 integration instead of 3×3 integration. The integration rule in thickness direction remains unchanged. It has to be noted again that the application of the SRI requires an isochoric-volumetric decoupled material law.

In this contribution an EAS approach, comparable to the second approach in section 3.4, is not included for the biquadratic elements. For this we refer to [6] and [7].

4.4 Trapezoidal locking

To avoid the trapezoidal locking effect for the biquadratic elements also an assumed strain interpolation for the normal strain in thickness direction is used. Therefore the biquadratic Lagrange functions

$$N_i(\xi,\eta) = \left(\frac{1}{2}\xi\xi_i\left(1+\xi\xi_i\right) + \left(1-\xi^2\right)\left(1-\xi_i^2\right)\right)$$

$$\left(\frac{1}{2}\eta\eta_i\left(1+\eta\eta_i\right)+\left(1-\eta^2\right)\left(1-\eta_i^2\right)\right)\ , \qquad i=1\ldots9\ . \tag{21}$$

are used as follows:

$$\begin{aligned}\tilde{\varepsilon}_{zz} \;=\;& N_{1(\xi,\eta)}\,\varepsilon_{zz(\xi_1=-1,\eta_1=-1)}+N_{2(\xi,\eta)}\,\varepsilon_{zz(\xi_2=1,\eta_2=-1)}+N_{3(\xi,\eta)}\,\varepsilon_{zz(\xi_3=1,\eta_3=1)}+\\ & N_{4(\xi,\eta)}\,\varepsilon_{zz(\xi_4=-1,\eta_4=1)}+N_{5(\xi,\eta)}\,\varepsilon_{zz(\xi_5=0,\eta_5=-1)}+N_{6(\xi,\eta)}\,\varepsilon_{zz(\xi_6=1,\eta_6=0)}+\\ & N_{7(\xi,\eta)}\,\varepsilon_{zz(\xi_7=0,\eta_7=1)}+N_{8(\xi,\eta)}\,\varepsilon_{zz(\xi_8=-1,\eta_8=0)}+N_{9(\xi,\eta)}\,\varepsilon_{zz(\xi_9=0,\eta_9=0)}\ .\end{aligned} \tag{22}$$

In analogy to the bilinear elements the strains ε_{zz} are the normal strains in thickness direction transformed to a local cartesian coordinate system.

4.5 Nomenclature

The nomenclature for the biquadratic elements is introduced in Table **2**. The only difference between the elements is due to the thickness interpolation. An additional extension -rv denotes selective **r**educed integration of the **v**olumetric terms, based on equation (12) and section 4.3, the extension -at denotes an **a**ssumed strain interpolation of the **t**ransverse normal strain following equation (22).

Elementname	biquadratic in-plane approximation	thickness approximation
MI9k3Dq	(17), (18)	(9)
MI9k3DEAS	(17), (18)	(3), (10)
xxx3Dyyy-rv	selective reduced integration of volumetric term, see (12)	
xxx3Dyyy-at	assumed strain interpolation of the transverse normal strain (22)	

Table 2: Nomenclature of the biquadratic elements.

5 ANALYTICAL STABILITY INVESTIGATIONS

In this section a single element under a homogenous compressions/tension state is investigated presuming a plane strain state, as such a loading combination proved to be critical for the elements and the behavior can be tested with a small number of degrees of freedom and deformation nodes. For this investigation only the linear elements are considered, for the biquadratic elements we refer to a forth coming paper. Because large deformations are treated in this example a linear elastic material law should no longer be valid, therefore a material of the Neo Hookean type is used.

5.1 Basics

The geometrical and material data are shown in figure (**2**). All nodes are fixed in z-direction, thus a plane strain case is generated. As a consequence of the boundary conditions shown in figure (**2**) the number of degrees of freedom for the whole system is reduced to eight.

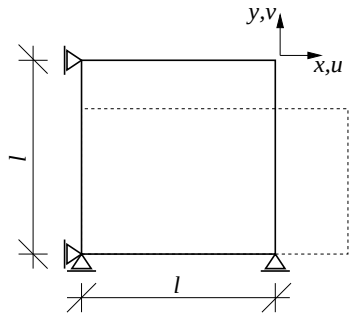

Geometry :

$$l = 2$$
$$t = 2$$

Neo Hooke material:

$$\kappa = 1.0 \cdot 10^5$$
$$\mu = 20$$

Uniform displacment in y-direction

Figure 2: Geometry and material data of the investigated element

For further simplification the upper four nodes are linked together in y-direction and as loading a uniform displacement v is prescribed for these nodes. As a nearly incompressible material is presumed, the displacement u for the nodes on the right hand side can be calculated approximately. The degree of conservation of the element volume is indicated through the determinant of the deformation gradient J, therefore for J a value between 0.999 for compression and 1.001 for tension is chosen to describe the incompressible material behavior. Thus the following equation for the displacement u is valid:

$$u = \frac{-1.9995v}{2+v}. \tag{23}$$

Using this expression it becomes possible to generate the displacement vector $\boldsymbol{d_e}$ with only one unknown variable u. Introducing the Matrix $\boldsymbol{D}$, which contains the shape functions, the element displacement can be represented as

$$\boldsymbol{u} = \boldsymbol{D}\,\boldsymbol{d}_e. \tag{24}$$

The axes of the given coordinate system are equal to the principal strain axes, thus the principal parts of the deformation gradient can be computed:

$$\lambda_1 = \frac{\partial \boldsymbol{u}}{\partial x} + 1 = \frac{\partial \boldsymbol{D}}{\partial x}\boldsymbol{d}_e + 1, \tag{25}$$

$$\lambda_2 = \frac{\partial \boldsymbol{u}}{\partial y} + 1 = \frac{\partial \boldsymbol{D}}{\partial y}\boldsymbol{d}_e + 1, \tag{26}$$

$$\lambda_3 = 1, \tag{27}$$

and the the principal stresses and the coefficients of the constitutive tangent tensor are obtained.

Consequently the Green Lagrange strain tensor is written directly as a function of the deformation gradient:

$$\boldsymbol{E} = \frac{1}{2}\left(\boldsymbol{F}^T\boldsymbol{F} - \boldsymbol{I}\right). \tag{28}$$

Finally the tangent stiffness matrix is given as:

$$\boldsymbol{K}^e_{tang} = \int_V \left(\boldsymbol{E}^T_{,\boldsymbol{d}_e}\boldsymbol{C}\boldsymbol{E}_{,\boldsymbol{d}_e} + \boldsymbol{E}^T_{,\boldsymbol{d}_e\boldsymbol{d}_e}\boldsymbol{S}\right) dV - \boldsymbol{L}^T_e\boldsymbol{P}^{-1}_e\boldsymbol{L}_e. \tag{29}$$

The matrices $\boldsymbol{L}_e$ and $\boldsymbol{P}_e$ appear, if the EAS method is applied. They include the constitutive tensor $\boldsymbol{C}$, the compatible strains $\boldsymbol{E}$ and the enhanced assumed strains $\boldsymbol{E}^{EAS}$:

$$\boldsymbol{L} = \int_V \boldsymbol{E}^{EAS^T}_{,\boldsymbol{\alpha}_e} \boldsymbol{C} \boldsymbol{E}_{,\boldsymbol{d}_e} dV, \tag{30}$$

$$\boldsymbol{P} = \int_V \boldsymbol{E}^{EAS^T}_{,\boldsymbol{\alpha}_e} \boldsymbol{C} \boldsymbol{E}^{EAS^T}_{,\boldsymbol{\alpha}_e} dV. \tag{31}$$

The terms (29), (30) and (31) are integrated with the standard $2\times2\times2$ Gauss integration. To avoid volumetric locking a selective reduced integration for the volumetric parts using $1 \times 1 \times 2$ Gauss points can be performed.

5.2 Eigenmodes

Because the number of degrees of freedom is reduced to four, only four eigenmodes have to be investigated. From these only the three eigenmodes represented in figure **3** are of any interest for the 'stability' considerations, whereas the fourth possible eigenmode always remains stable, resp. has always a positiv eigenvalue.

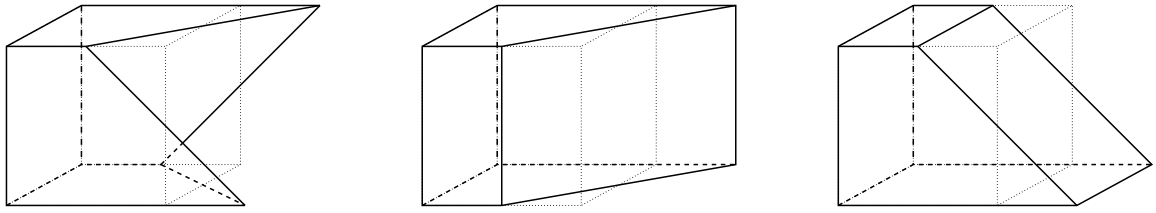

mode 1 mode 2 mode 3

Figure 3: Investigated eigenmodes of 8-node-element

5.3 Results

Figure **4** shows that using a pure displacement formulation the investigated eigenvalues remain stable. If in addition selective reduced integration is applied for the volumetric parts the eigenvalues of mode 1 and mode 2 become very small. This was expected, because locking effects should be obviated. Nevertheless, the eigenvalues still remain in the positive range, even for high compression.

In figure **4** and **5** the eigenvalues are depicted for the displacement formulation combined with the ANS-method. It is clearly visible that for the ANS3DL element the eigenmodes 1 and 2 become unstable in the case of very large compressive strains. But it must also be noted that this state of about 90% compression is hardly found in a realistic problem. If in addition selective reduced integration of the volumetric parts is applied the eigenvalues of mode 1 and mode 3 become very small for the complete deformation range and mode 1 is appearing at about 75% compression.

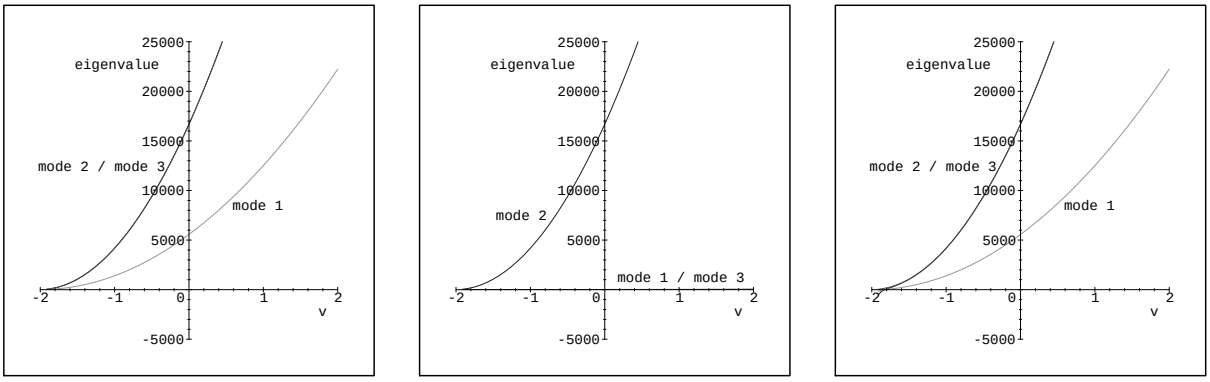

Figure 4: Eigenvalues of Eigenmodes 1, 2 and 3 as a function of the deformation v in y-direction; DISP3D element (left side) and DISP3D-rV element (middle); ANS3DL element (right side); + tension, - compression

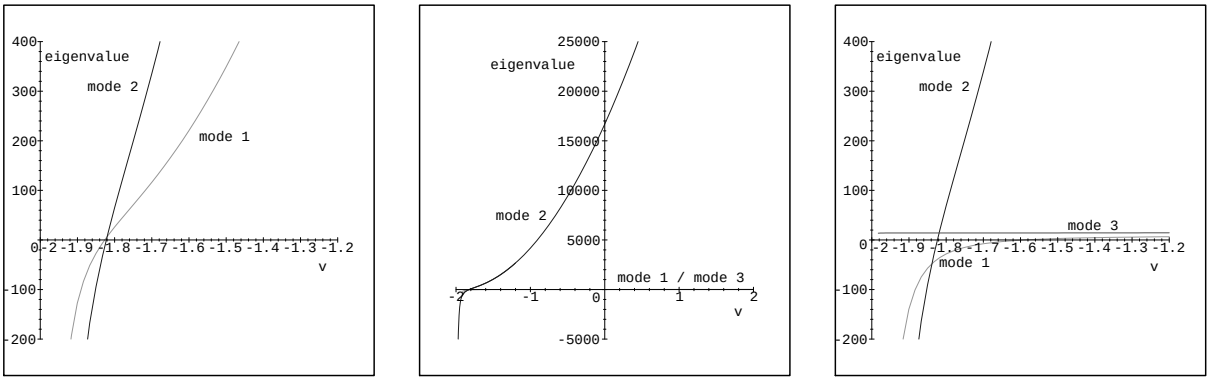

Figure 5: Eigenvalues of Eigenmodes 1, 2 and 3 as a function of the deformation v in y-direction; ANS3DL element (zoomed to $-2.0 < v < -1.2$ on left side); ANS3DL-rV element (full range in the middle and zoomed to $-2.0 < v < -1.2$ on right side)

In the ANS3DEAS element an enhanced assumed strain interpolation is added for the strains in thickness direction (Figure **6**). This enhancement leads to unstable modes 1 and 2 at compressive loading of lower value than the ANS3DL element and additionally the eigenvalue of mode 1 becomes very small for the complete deformation range considered. A small eigenvalue for mode 3 is obained, too, if selective reduced integration of the volumetric parts is used in addition.

If the EAS-method is further applied to enhance the inplane strains, hourglassing starts already at a compression of about 45% (see figure **7**). If selective reduced integration of the volumetric parts is used for the eas**-elements, the hourglass eigenmode is also present in the tension case, in a similar deformation range as for compression. In general, all eigenvalues are rather small for this combination of element enhancements.

Similar observations have been made for the biquadratic elements. As a conclusion

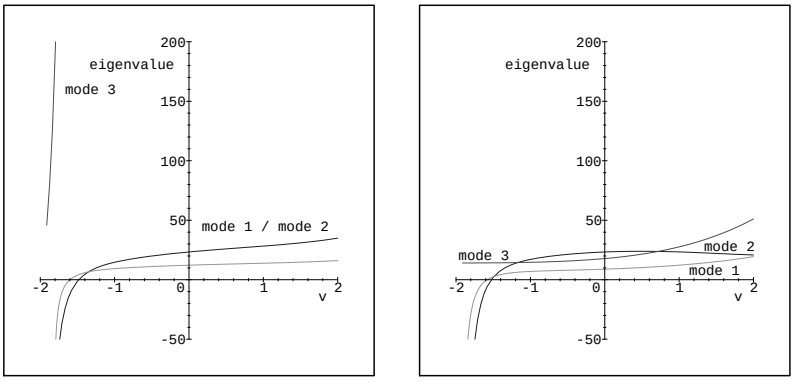

Figure 6: Eigenvalues of Eigenmodes 1, 2 and 3 as a function of the deformation v in y-direction; ANS3DEAS element (left side) and ANS3DEAS-rV element (right side)

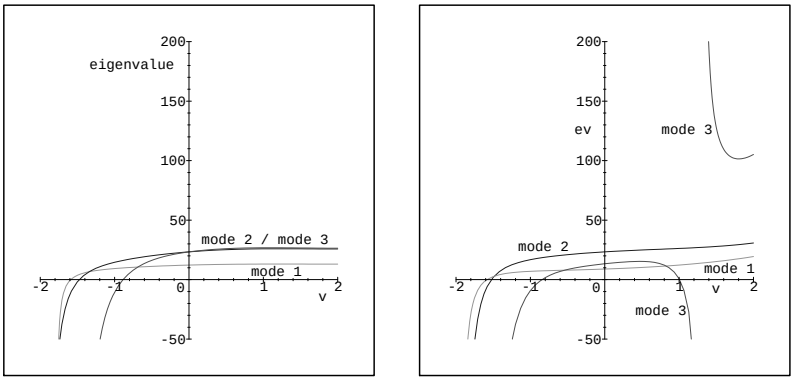

Figure 7: Eigenvalues of Eigenmodes 1, 2 and 3; eas3DEAS element (left side) and eas3DEAS-rV element (right side)

it must be noted that all mixed type enhancements of the low order interpolated solid-shell elements lead to artificial element kinematics under homogenous loading in the large deformation regime.

6 NUMERICAL EXAMPLES

The following numerical analyses are performed with 8-node and 18-node hexahedron elements with bilinear resp. biquadratic inplane interpolation.

6.1 Bending problem with distorted director angle

In this section a cantilever beam is investigated varying the angle for an element edge director and normals. The geometry and material data are given in figure **8**. These investigations were performed using all present types of element formulations. The angle Θ was varied between 0^o resp. 45^o. The results are presented in table **3**.

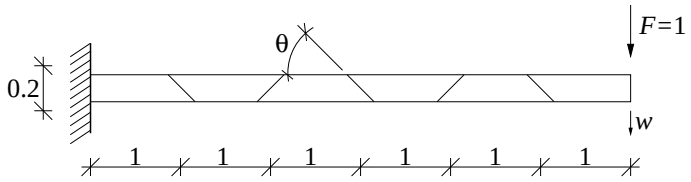

$$E = 1.0 \cdot 10^6$$
$$\nu = 0.0/0.3$$
$$\Theta = 0^o/45^0$$

Figure 8: Geometry, boundary conditions and material data of the cantilever beam

The trapezoidal locking effect is clearly visible for the elements without modification to avoid trapezoidal locking, independent of the in-plane interpolation. If an angle of $\Theta = 45^o$ is chosen the displacement w is only between 14 and 23% of the displacement obtained for an angle of $\Theta = 0^o$. It is also visible from table **3** that the interpolation of the normal strain in thickness direction, as specified in eqn. (16) and (22), eliminates the locking effect completely.

displacement w	$\Theta = 0^o$ $\nu = 0.0$	$\Theta = 0^o$ $\nu = 0.3$	$\Theta = 45^o$ $\nu = 0.0$	$\Theta = 45^o$ $\nu = 0.3$
ANS3DEAS	0.1073	0.1073	0.0166	0.0156
EAS3DEAS	0.1073	0.1073	0.0166	0.0159
eas3DEAS	0.1073	0.1073	0.0166	0.0159
ANS3Dq	0.1073	0.1071	0.0167	0.0147
eas3Dq	0.1073	0.1071	0.0167	0.0151
MI9k3DEAS	0.1081	0.1064	0.0244	0.0235
MI9k3Dq	0.1081	0.1064	0.0244	0.0236
ANS3DEAS-at	0.1073	0.1073	0.1074	0.1072
EAS3DEAS-at	0.1073	0.1073	0.1074	0.1072
eas3DEAS-at	0.1073	0.1073	0.1074	0.1072
ANS3Dq-at	0.1073	0.1071	0.1074	0.1071
eas3Dq-at	0.1073	0.1071	0.1074	0.1071
MI9k3DEAS-at	0.1081	0.1065	0.1076	0.1061
MI9k3Dq-at	0.1081	0.1064	0.1076	0.1061

Table 3: Deflection of a cantilever beam for varied director angles $\Theta = 0^o$ and $\Theta = 45^o$ and different Poisson ratio.

6.2 Square plate undergoing large elastoplastic deformations

In this section a square plate which is subjected to uniform loading q_0 (deadload) with the geometry and material data given in figure **9** is analyzed. The material behavior is described by the Hencky material law for the elastic part with von Mises plasticity. This problem is chosen to compare the behavior of the different elements for large deformations involving plasticity.

At the edges the lower boundary of the plate is fixed in vertical direction whereas the

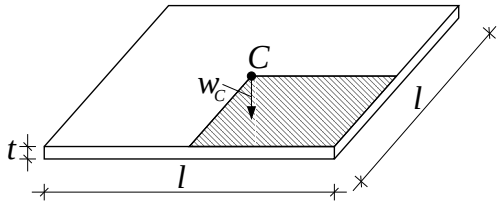

Geometry:			Material:		
l	=	508	κ	=	57500
t	=	2.54	μ	=	26538
Loading:			y_0	=	248
q_0	=	10^{-2}			

Figure 9: Square plate geometry, material data and loading

displacements tangential to the plate and the upper boundary are free.

Due to symmetry only a quarter of the plate is discretized with 1 element over the thickness and 32x32 elements in tangent plane for the bilinear elements. Using the biquadratic elements the structure is discretized with a mesh of 16x16 elements only. For the integration in thickness direction six Gauss points are used.

As expected the curves for the center displacement - depicted in figure **10** - coincide for displacements smaller than about $w_C = 25$ whereas full integration of the volumetric terms leads to a clearly stiffer behavior in the larger displacement range. This is a consequence of the incompressibility locking occurring in the plastic zones. The enhancement of the in-plane strains included in the EAS3DEAS element and the eas3DEAS element is responsible for the first visible differences in the results, with little difference between the results for the different in-plane enhancements. It becomes also apparent that even

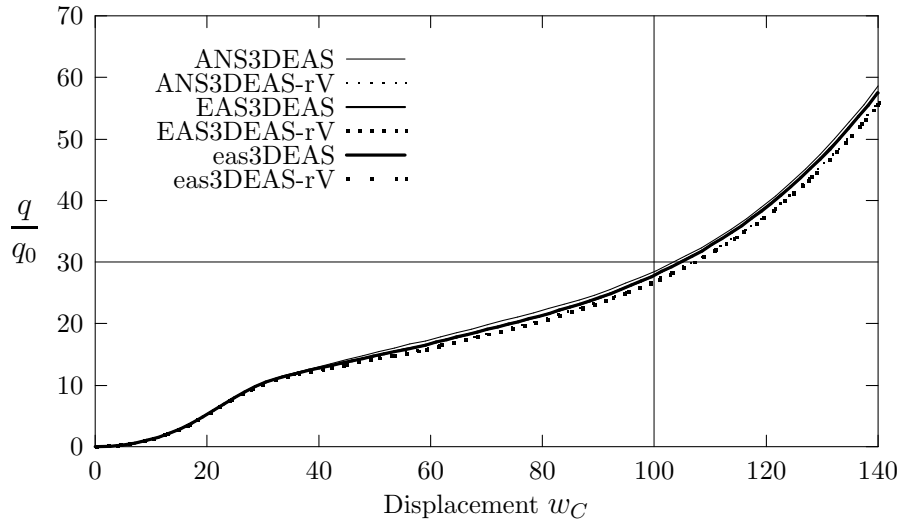

Figure 10: Square plate; load deflection diagram; displacement of center point for 'bilinear' solid shell elements with different enhancements

the 6-parameter enhancement (eas..) does not remove the volumetric locking completely. Selective reduced integration leads to almost coincident results for all 8-node solid shells. All the mentioned effects are more pronounced for coarser - non converged - meshes.

The results obtained with 16x16 'biquadratic' 18-node elements are very close to the results obtained with 32x32 'bilinear' 8-node elements depicted in figure **11**. There appears

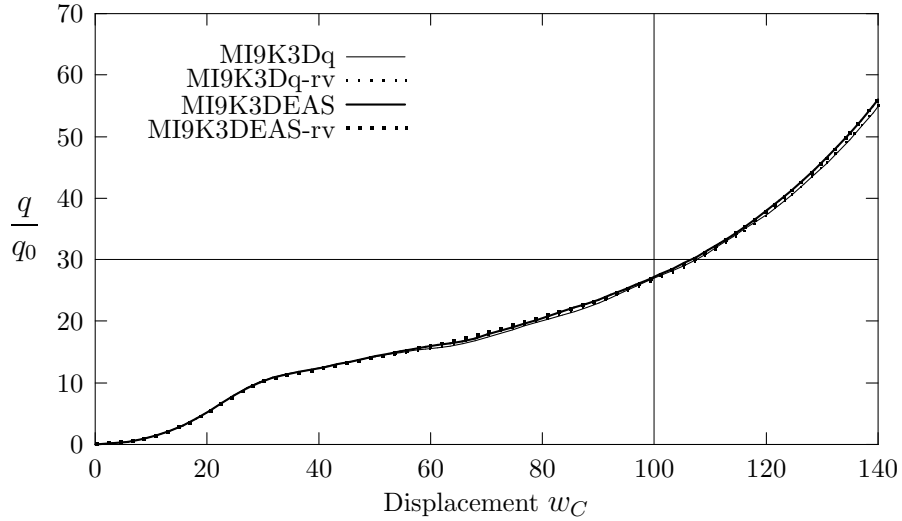

Figure 11: Square plate; load deflection diagram; displacement of center point for 'biquadratic' solid shell elements with different enhancements

to be no volumetric locking effect for the 'biquadratic' elements in this example.

7 CONCLUSIONS

Various approaches to avoid volumetric locking in the case of incompressibility were presented for the solid-shell concept, concerning the influence of the different enhancements the behavior of the solid-shell elements with bilinear form functions was compared to the behavior of solid-shell elements with biquadratic form functions. The latter are known to provide better results for curved structures.

Concerning volumetric locking it was shown that enhancements of the in-plane strains according to the enhanced assumed strain method for the 'bilinear' type elements do not lead to a complete locking removal. The elements with selective reduced integration of the volumetric term appear to deliver better results in such cases without leading to any kinematics.

The example of the cantilever beam with a distorted element mesh shows clearly the effect of so-called trapezoidal locking and the complete removal of this effect using an assumed strain interpolation for the normal strain in thickness direction.

It should also be noted that using the EAS-method - as known from Wriggers/Reese [22] - as well as using the selective reduced integration of volumetric parts can lead to artificial unstable eigenmodes of the investigated structure under some kinds of loading in the case of large deformations. Even the enhancement with the ANS-method leads to artificial unstable eigenmodes in some cases. Future developments are directed to a proper method to eliminate these unstable eigenvalues. Different proposals to resolve such problems are already suggested in the literature [11], [13], [21] and [29], however they all appear not to be generally applicable.

REFERENCES

[1] K. J. Bathe and E. Dvorkin, 'A continuum mechanics based four-node shell element for general nonlinear analysis', *Eng. Comput.* **1**, 77-88 (1984).

[2] J. L. Batoz, 'On 8-node solid elements for linear and nonlinear analysis of shell undergoing large rotations but small strains', *Euromech Colloquium 371*, Karlsruhe, Germany, 1997.

[3] P. Betsch and E. Stein, 'An assumed strain approach avoiding artificial thickness straining for a non-linear 4-node shell element', *Communications in Numerical Methods in Engineering*, Vol.11, 899-909 (1995).

[4] D. Braess, 'Enhanced assumed strain elements and locking in membrane problems' *Comput. Methods Appl. Mech. Engrg.* **165**, 155-174 (1998)

[5] M. Braun, *Nichtlineare Analysen von geschichteten elastischen Flächentragwerken*, Bericht Nr. 19, Institut für Baustatik, Universität Stuttgart, 1995.

[6] M. Bischoff, E. Ramm and D. Braess, 'A class of equivalent enhanced assumed strain and hybrid stress finite elements', *Computational Mechanics* **22**, 443-449 (1999).

[7] M. Bischoff, *Theorie und Numerik einer dreidimensionalen Schalenformulierung*, Institut für Baustatik, Universität Stuttgart, Dissertation, 1999.

[8] N. Büchter and E. Ramm, '3D-extension of nonlinear shell equations based on the enhanced assumed strain concept', in Ch. Hirsch, J. Periaux and E. Onate (eds.), *Computational Methods in Applied Sciences*, Amsterdam, 1992.

[9] E.N. Bucalem and K.J. Bathe, 'Higher-order MITC general shell elements', *Int. J. Numer. Meth. Engng.* **36**, 3729-3754 (1993).

[10] S. Doll, *Zur numerischen Behandlung großer elasto-viskoplastischer Deformationen bei isochor-volumetrisch entkoppeltem Stoffverhalten*, Institut für Mechanik, Universität Karlsruhe, Dissertation, 1998.

[11] S. Doll, R. Hauptmann, C. Freischläger and K. Schweizerhof, 'On volumetric locking of low-order Solid and Solid-Shell Elements for Finite elastoviscoplastic Deformations', submitted for publication (2000).

[12] R. Eberlein, *Finite-Elemente-Konzepte für Schalen mit großen elastischen und +plastischen Verzerrungen*, Fachbereich Mechanik, Technische Hochschule Darmstadt, Dissertation, 1997.

[13] S. Glaser, F. Armero 'On the formulation of enhanced strain finite elements in finite deformations' *Engineering Computations*, Vol.14 No.7, 759-791 (1997)

[14] F. Gruttmann, *Theorie und Numerik dünnwandiger Faserverbundstrukturen*, Bericht Nr. F96/1, Institut für Baumechanik und Numerische Mechanik, Universität Hannover, 1996.

[15] R. Hauptmann, *Strukturangepaßte geometrisch nichlineare Finite Elemente für Flächentragwerke*, Institut für Mechanik, Universität Karlsruhe, Dissertation, 1997.

[16] R. Hauptmann and K. Schweizerhof, 'A systematic development of solid-shell element formulations for linear and nonlinear analyses employing only displacement degrees of freedom', *Int. J. Numer. Methods Engng.* **42**, 49-70 (1998).

[17] R. Hauptmann, K. Schweizerhof and S.Doll, 'Extension of the solid-shell concept for large elastic and large elastoplastic deformations', accepted by *Int. J. Numer. Methods Engng.* (1998).

[18] R. Hauptmann, S. Doll, M. Harnau and K. Schweizerhof, "Solid-shell' elements with linear and quadratic shape functions at large deformations with nearly incompressible materials', to appear.

[19] J.C. Nagtegaal, D.M. Parks and J.R. Rice, 'On numerically accurate finite element solutions in the fully plastic range', *Comp. Meth. Appl. Mech. Engng.* **4**, 153-177 (1974).

[20] H. Parisch, 'A continuum-based shell theory for non-linear applications', *Int. J. Num. Methods Engng.* **38**, 1855-1883 (1995).

[21] S. Reese, M. Kuessner, B.D. Reddy 'A new stabilization technique for finite elements in non-linear elasticity', *Int. J. Num. Methods Engng.* **44** 1617-1652 (1999)

[22] S. Reese and P. Wriggers *A stabilization technique to avoid hourglassing in finite elasticity*, Report No. 4/98, Institute of Mechanics TU Darmstadt, Germany

[23] C. Sansour, 'A theory and finite element formulation of shells at finite deformations involving thickness change', *Archive of Applied Mechanics* **65**, 194-216 (1995).

[24] B. Seifert, *Zur Theorie und Numerik Finiter elastoplastischer Deformationen von Schalenstrukturen*, Bericht Nr. F96/2, Institut für Baumechanik und Numerische Mechanik, Universität Hannover, 1996.

[25] J.C. Simo and M.S. Rifai, 'A class of mixed assumed strain methods and the method of incompatible modes', *Int. J. Numer. Methods Engng.* **29**, 1595-1638 (1990).

[26] J.C. Simo, R.L. Taylor and K.S. Pister, 'Variational and projection methods for volume constraint in finite deformation elasto-plasticity', *Comp. Meth. Appl. Mech. Engng.* **51**, 177-208 (1985).

[27] K.Y. Sze 'Trapezoidal locking and solid-shell formulations', Presentation at Oberwolfach Meeting on: *Mathematische Annalyse von FEM für Probleme in der Mechanik*, March 1999

[28] H. Verhoeven, *Geometrisch und physikalisch nichtlineare finite Plattenelemente mit Berücksichtigung der Dickenverzerrung*, Dissertation, Reihe Maschinenbau, Technische Universität Berlin, 1992.

[29] W.A. Wall, M. Bischoff and E. Ramm 'Stabilization techniques for fluid and structural finite elements', IACM world congress *Computational Mechanics* CIMNE, Barcelona, Spain 1998

[30] E.L. Wilson, R.L. Taylor, W.P. Doherty and J. Ghaboussi, 'Incompatible displacement models', In: Numerical and Computational Methods in Structural Mechanics, S.T. Fenves et al. eds., Academic Press, 43-57 (1973).